Pré-Publicações do Departamento de Matemática
Universidade de Coimbra
Preprint Number 12–18

CONTROLLED DRUG DELIVERY AND OPHTHALMIC APPLICATIONS

J.A. FERREIRA, P. DE OLIVEIRA AND P. M. DA SILVA

Abstract: The goal of this paper is to present an overview of drug delivery from polymeric therapeutic lens to the anterior segment of the eye. Mathematical models that describe *in vitro* and *in vivo* drug delivery, from different types of lens, are presented. Healthy and pathological situations are addressed. Numerical simulations are included and compared with experimental results.

Key words: Controlled drug delivery, effective time, therapeutic lens, mathematical model, partial differential equations.

Mathematics Subject Classification (2000): 35B30, 35K99

1. Introduction

Controlled drug delivery occurs when a polymer is combined with a drug in a such a way that the release profile is predefined. Conventional forms of drug delivery are based on tablets, eye drops, ointments and intravenous solutions. These delivery systems were characterized by an immediate and non controlled kinetics depending essentially on the properties of tissues to absorb drugs.In the last decades drug delivery devices have moved to more complex controlled systems. Advances in polymer science have led to the development of second generation drug-delivery systems which purpose is to maintain drug concentration in the blood or in target tissues at a desired value and during an extended period of time. The improvements in the properties of polymers, by combining different compounds and additives, the use of biodegradable polymers and the enhancement of diffusion processes come at the expense of more complex transport phenomena which are known to influence drug delivery rates. The urgency for mathematical models in the area and the necessity for a predictive environment, avoiding costly in vitro experiments, become all the more relevant in light of the heightened focus on polymer-based drug-delivery devices. Also future drug delivery modelling work should consider drug transport in target tissues after its release from polymeric devices.

Received May 25, 2012.

Efficient drug delivery to the eye is becoming increasingly vital with the development of new devices and the increasing prevalence of eye diseases, accompanying population ageing .In this paper we will present an overview of drug delivery from therapeutic lens to the anterior segment of the eye. The platforms we analyse and the models we present to simulate the drug release can be easily adapted to the case of transdermal drug delivery systems.

The eye is anatomically divided into the anterior and posterior segments with the lens-iris barrier roughly demarcating the two segments. For both the anterior and the posterior segment of the eye, topical route is very inefficient in delivering therapeutic concentrations because of drainage through the naso-lacrimal ducts, low permeability of corneal epithelium, systemic absorption and the blood aqueous barrier. According to these facts it is estimated that when a drop is instilled into the eye it is diluted by the lacrimal secretion and 95% is cleared by the tear fluid. To avoid drug loss, side effects and also to improve the efficiency of drug delivery, many researchers have proposed the use of therapeutic contact lenses as a vehicle to deliver ophthalmic drugs. The main advantage of this method is the possibility of controlling the drug delivery by means of the use of polymeric matrices designed to achieve pre-defined performances as well as their high degree of comfort and biocompatibility. Several techniques have been proposed in the literature. Without being exhaustive we can mention the use of

(i) soaked simple contact lenses ([1], [2], [3]);
(ii) compound contact lenses with a hollow cavity ([4]);
(iii) entrapment of drugs by polymerization of hydrogel monomers in the presence of species to be entrapped or by direct dissolution ([5], [6], [7], [8], [9], [10], [11], [12]);
(iv) biodegradable contact lenses ([13]).

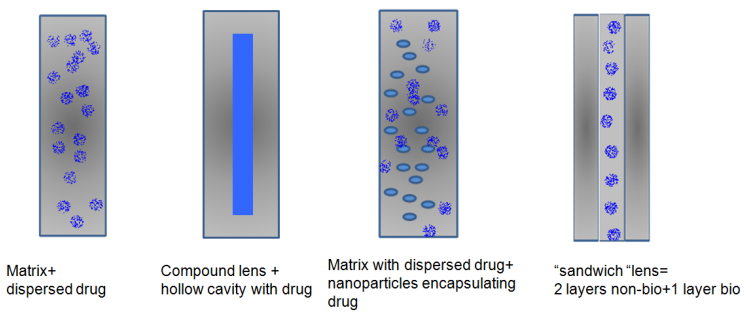

FIGURE 1. Examples of single and multilayer drug delivery systems.

The use of soaked simple lens is more efficient than the use of ophthalmic drops but the drug loading is very limited and the delivery period of time is very short. In the case of lens with an hollow cavity it has been observed that the oxygen and carbon dioxide permeability is lower than the prescribed for a safe daily use. In [6] and [7] the entrapment of the drug is achieved by polymerization of monomers and by encapsulation of drug within particles dispersed in the lens. The nanoparticles are formed by polymerization, during or after which the drug is added, leading to covalent drug binding to the polymer. This binding of the drug depends on its physicochemical properties as well as the nature of the polymer.

In the case of encapsulation in particles the drug to be delivered must overcome two barriers: the diffusion in the particles and the diffusion in the polymeric matrix. As a consequence the drug release attains in this case several days.The main difference between the lens proposed in [6] and [8] lies in the polymers used: in [6] the polymeric matrix was made from a p-HEMA [*] gel whereas in [8] the film was prepared using p-HEMA/MAA [†] ; the particles in [6] were stabilized with a silica shell and in [8] silicone particles have been used. In the case of [6] there is a delay period between the delivery from the polymeric matrix and from the particles. It can attain three or four days and during this period there is practically no drug delivery. In [8] the drug is continuously delivered with no pause period during the release.

At the best of our knowledge the more recent type of therapeutic lens has been proposed by a team of Harvard Medical School in [13]. The idea underlying the mechanism used to induce a delay in the drug delivery is to use a sandwich type structure composed by three polymeric layers as represented in Figure 1: two non biodegradable layers(HEMA) coating a biodegradable PLGA [‡] film containing drug. Numerical simulations of drug delivery from the lens in [8] and in [13] have been compared in [14]. According to the numerical simulations presented there and to in vitro experiments reported in [13] the release from the "sandwich lens" is slower than the release from therapeutic lens presented in [8] and [6], lasting for thirty days.

From a medical point of view, the central question is to have a prediction of the drug concentration in the anterior chamber of the eye. In this

[*]Monomer 2-hydroxyethyl methacrylate

[†]Copolymer 2-hydroxyethyl methacrylate co-methacrylic acid

[‡]Copolymer poly lactic co-glycolic acid

case mathematical models are the only available tool to make such prediction. Mathematical models describing the behaviour of drug concentration across the cornea when a drop is instilled were proposed in [15], [16] and [17]. Nevertheless, when the drug is delivered from a contact lens the concentration and mass profiles across the cornea are qualitatively different. In [9] a mathematical model to predict drug concentration in the anterior chamber when the drug is delivered from a therapeutic contact lens, where the drug is dispersed in the polymeric matrix and encapsulated in nanoparticles, has been presented. A comparison with the behavior of concentration plots in the anterior chamber, in the case of topical drug administration, shows the efficiency of controlled drug delivery.

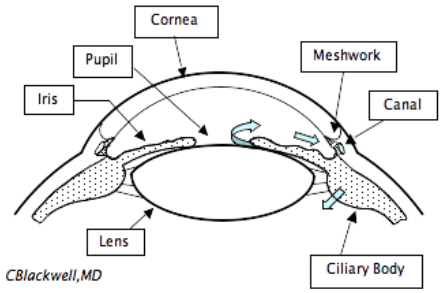

FIGURE 2. Anatomy of the eye (http://www.blackwelleyesight.com/narrated-eye-exam/).

Therapeutic lens are essentially used in the case of severe diseases as glaucoma, for which long periods of drug delivery, from one week to a month, are needed. Glaucoma is related with a buildup of intraocular pressure (I.O.P.) due to an obstruction of Schlemm canals or an excessive production of aqueous humor (Figure 2). In [9] the delivery in the anterior chamber was modelled by an ordinary differential equation, and consequently its anatomy was not taken into account. To obtain a more realistic description of the delivery, the I.O.P. and the physio-pathological characteristics of the anterior chamber should be considered. To describe the *in vivo* delivery a mathematical model which consists of three coupled systems linked by interface conditions was considered: drug delivery from a therapeutic lens, diffusion and metabolic consumption in the cornea, diffusion, convection and metabolic consumption in the anterior chamber of the eye. Numerical simulations in healthy and

pathological conditions can be of great help to ophthalmologists and to material scientists because they give indications of how to tailor polymeric lens to fit specific patient's needs.

In Section 2 we present two mathematical models that simulate *in vitro* drug delivery from the lens in [8] and the lens in [13]. Comparisons with laboratorial experiments are also presented. For the lens with particles a time constant which represents the mean time to achieve equilibrium -effective time ([18], [19])- is computed. In Section 3 we present a mathematical model that simulates *in vivo* drug delivery to the anterior chamber from a therapeutic lens ([20]). Numerical simulations in healthy and pathological conditions are analysed. In Section 4 some conclusions are addressed.

2. Simulating *in vitro* drug release from therapeutic lens

In this Section we will focus mainly on two types of therapeutic lens: lens with dispersed particles encapsulating drug ([8]) and sandwich type lens ([13]).

2.1. Lens with particles.

2.1.1. *Mathematical model and laboratorial experiments.* The lens is a p-HEMA/MAA platform with flurbiprofen dispersed and entrapping particles filled with drug ([8]). The copolymers with drug incorporated in the polymeric matrix were synthesized by dissolving flurbiprofen directly into the mixture of monomers and adding a microemulsion containing silicone particles encapsulating drug. The solution was injected into a mold, constituted by two glass plates coated with teflon. The polymerization reaction was performed at 60º C during 24 hours. The obtained copolymer was cut into circular samples with 1 cm of diameter. A complete description of materials and methods used can be found in [8].

In Figure 3 we present a SEM (scanning electron microscopy) micrograph of a copolymer with drug dispersed and particles encapsulating drug ([8]).

The mathematical model used to simulate *in vitro* drug delivery (when the lens has a width of 2ℓ and is completely immersed in water) which we denote by model I, is represented by the system of partial differential equations

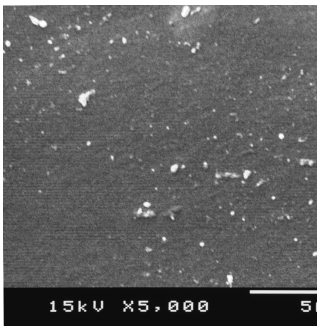

FIGURE 3. SEM image of the cross section of a copolymer with particles.

$$\begin{cases} \dfrac{\partial C^g}{\partial t} = D\dfrac{\partial^2 C^g}{\partial x^2} - \dfrac{\partial C^b}{\partial t}, x \in (-\ell, \ell), t > 0 \\ \dfrac{\partial C^b}{\partial t} = \lambda(C^g - C^b), x \in (-\ell, \ell), t > 0 \end{cases}, \tag{1}$$

where C^g represents the drug concentration in the gel, C^b the drug concentration in the particles, D the diffusion coefficient of the drug in the gel and λ stands for the product of the mass transfer coefficient for drug transport across the particle surface and the ratio between the surface and the volume of particles.

System (1) is completed with the initial conditions

$$\begin{cases} C^g(x,0) = C^{0g} \\ C^b(x,0) = C^{0b} \end{cases}, \tag{2}$$

where C^{0g} is the initial concentration in the gel and the C^{0b} the initial concentration inside the particles, and the boundary conditions

$$\begin{cases} C^g(-\ell, t) = C^E \\ \\ C^g(\ell, t) = C^E \end{cases}, \tag{3}$$

with C^E representing an external concentration. Alternatively flux boundary conditions of type

$$\begin{cases} D\dfrac{\partial C^g}{\partial x}(-\ell, t) = \alpha_1(C^g(-\ell, t) - C^E),\ t > 0 \\ -D\dfrac{\partial C^g}{\partial x}(\ell, t) = \alpha_1(C^g(\ell, t) - C^E),\ t > 0 \end{cases} \tag{4}$$

can be considered, where α_1 stands for a transference coefficient. We note that (4) is a more realistic description of the clearance mechanisms, meaning that the drug flux at the boundary of the lens is proportional to the difference between the drug concentration in the exterior region and the drug concentration at the lens surface. Conditions (3) mean that the drug is immediately removed and the external drug concentration is constant. To simulate in laboratory this behaviour the concentration of drug in water is kept constant by means of a renewal mechanism that takes place at fixed intervals of time.

Due to the linearity of (1) an exact solution for the total released mass $M(t)$ can be computed. Using for a sake of simplicity conditions (3) we obtain after some tedious but straightforward computations ([8])

$$M(t) = -\frac{4D}{\ell}\sum_{n=0}^{\infty}\frac{C^E(a_n+2\lambda)-C^{0g}(a_n+\lambda)-\lambda C^{0b}}{a_n(a_n^2+2\lambda^2+2a_n\lambda)}(a_n+\lambda)(e^{a_n t}-1), \quad (5)$$

where $a_n = \dfrac{-8\lambda\ell^2 - D(2n+1)^2\pi^2 \pm \sqrt{(8\lambda\ell^2)^2 + D^2(2n+1)^4\pi^4}}{8\ell^2}, n = 0, 1, \ldots$.

To have a clear picture of the delay effect of particles different scenario were considered(Table I).

Table I: Description of the Systems of Model I.

Systems	Definition	Parameters
System 1	matrix with dispersed drug	$C^{0b} = 0$, $\lambda = 0$
System 2	matrix with silicone particles encapsulating drug	$C^{0g} = 0$, $\lambda \neq 0$
System 3	matrix with dispersed drug and entrapped in particles	$C^{0b} = C^{0g}$, $\lambda \neq 0$
System 4	matrix with dispersed drug and void particles at $t = 0$	$C^{0b} = 0$, $\lambda \neq 0$

System 3 represents the lens in [8]. System 4 describes an academic situation used to test the robustness of the model.

Using $C^E = 0$, $D = 0.05$, $\lambda = 0.05$ and the information in Table I, it can be proved analytically, from (5) that for any choice of the parameters

$$M_2(t) < M_3(t) < M_4(t) < M_1(t),\ t > 0, \quad (6)$$

where M_i, $i = 1, 2, 3, 4$ represent delivered mass for Systems 1, 2, 3 and 4 respectively. In Figure 4 we exhibit plots computed from the analytical solution (5) considering one hundred terms. We took $C^{0b} = 0.5$ for $M_2(t)$ and

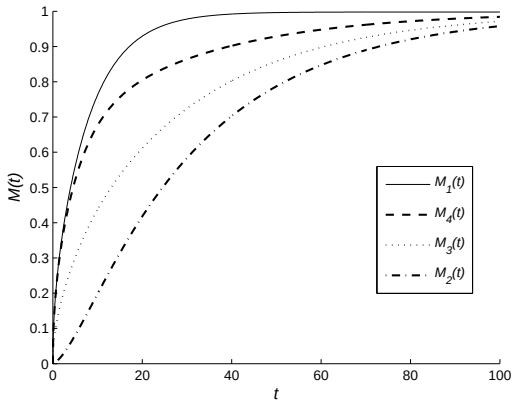

FIGURE 4. Delay effect on the drug release of the particles for Systems 1, 2, 3 and 4.

$C^{0g} = 0.5$ for $M_1(t)$ and $M_4(t)$. For $M_3(t)$ we considered $C^{0g} = C^{0b} = 0.25$. We note that the values of the parameters used in the simulations of Figure 4 are not physical.

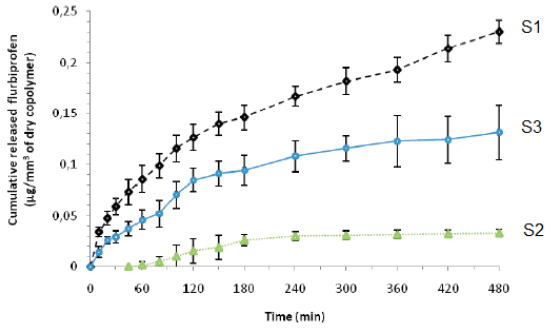

FIGURE 5. Experimental release profiles of flurbiprofen for three different platforms.

In Figure 5 we exhibit experimental release profiles of flurbiprofen for Systems 1, 2 and 3 (S1, S2, S3). At this point we just want to underline the qualitative agrement between numerical results in Figure 4 and experimental results in Figure 5. In what follows physical parameters will be considered in the simulations.

2.1.2. *Mean time to achieve equilibrium: effective time constant.* To improve the design of the lens it is important to know the waiting time that is the

period of time elapsed before the mass attains a certain therapeutic level and how to adjust the parameters to produce a pre-defined delivery profile. In this subsection we compute the effective time ([18]).

Let M^s represents the steady mass that is $M^s = \lim_{t\longrightarrow\infty} M(t)$. The effective time t_{eff} is defined as the mean time to achieve the equilibrium,

$$t_{eff} = \frac{\int_0^\infty t(M^s - M(t))dt}{\int_0^\infty (M^s - M(t))dt}, \tag{7}$$

which can be seen as the first moment of the probability density function

$$d(t) = \frac{M^s - M(t)}{\int_0^\infty (M^s - M(t))dt}. \tag{8}$$

To compute t_{eff} only $\overline{M}(p)$, the Laplace transform of $M(t)$, must be known. In fact it can be proved ([18], [19]) that if $\overline{M}(p)$ can be expanded in powers of p,

$$\overline{M}(p) = \frac{1}{p}(B_1 + B_2 p + B_3 p^2 + ...), \tag{9}$$

then

$$t_{eff} = -\frac{B_3}{B_2},$$

provided that $B_2 \neq 0$.

In the case $D \neq 0$, $\lambda \neq 0$, we give $\overline{M}(p)$ the form (9), with

$$B_1 = -2a\frac{\ell}{\lambda},\ B_2 = \frac{\ell}{\lambda}(\frac{a}{\lambda} + \frac{4a}{3D}\ell^2 - 2\varpi),$$

$$B_3 = \frac{\ell}{\lambda}(-\frac{4a}{3\lambda D}\ell^2 - \frac{16a}{15D^2}\ell^4 + \frac{2}{\varpi}\lambda + \frac{4\varpi}{3D}\ell^2 - \frac{a}{\lambda^2} + \frac{\varpi}{\lambda}),$$

where

$$a = 2\lambda C_{ext} - \lambda(C^{0g} + C^{0b}), \varpi = \frac{C^{0b} - C^{0g}}{2}.$$

After some tedious but straightforward computations we obtain ([12])

$$t_{eff} = \frac{1}{\lambda D}\frac{2\varpi D^2\lambda - aD^2 - \frac{4}{3}a\lambda D\ell^2 - \frac{16}{15}a\lambda^2\ell^4 + \frac{4}{3}\varpi D\lambda^2\ell^2}{2\varpi D\lambda - aD - \frac{4}{3}a\lambda\ell^2}. \tag{10}$$

In the case of System 1 ($\lambda = 0$, $C^{0b} = 0$), effective time can not be obtained from (10). A direct calculus from (9) leads to

$$t_{eff} = \frac{2\ell}{5D}. \tag{11}$$

In Figure 6 plots of t_{eff} given by (10), as a function of λ and D, are exhibited with $C^{0g} = 0.5$, $C^{0b} = 0.25$, $C_{ext} = 0$, $\ell = 1$. As expected effective time is a decreasing function of D, for constant λ, and a decreasing function of λ, for constant D. In fact when D increases the drug diffuses faster; when λ increases the drug encapsulated in the particles easier surmounts the barrier represented by their boundary. We note that the influence of D is more significant than the influence of λ.

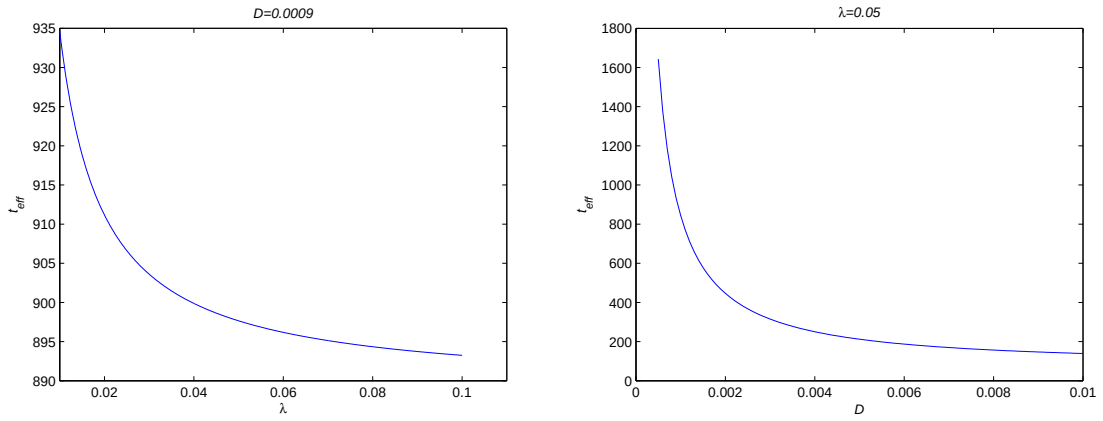

FIGURE 6. Behavior of t_{eff} as a function of λ (left) and D (right).

In engineering literature ([19]) it is generally accepted that the onset of equilibria is defined by the response time t_r, where $t_r = 4t_{eff}$. We presented an explanation of this assumption in [21].

If we compute $4t_{eff}$ for the previous systems, for $D = 0.05$, $\ell = 1$, $\lambda = 0.05$, $C^{0g} = 0.5$, $C^{0b} = 0.5$, $C_{ext} = 0$, we obtain the values presented in Table II.

Table II - Response times of model I.

	System 1	System 2	System 3	System 4
$4t_{eff}$	32	121.6	116.5716	104

We note that $t_r^1 < t_r^4 < t_r^3 < t_r^2$, where the superscript refers to the systems. This result agrees with the inequalities established in (6) for the delivered masses. In fact if for example $M_2(t) < M_3(t)$ than the steady state of System 2 is reached after the steady state of System 3, that is $t_r^3 < t_r^2$. We observe that System 2 induces the largest delay. However it can not be used as a platform of drug delivery because the loading of particles still presents many laboratorial problems.

Interpreting t as a statistical variable, with exponential density distribution $d^*(t)$, the probability that $t \leq kt_{eff}$, $P(t \leq kt_{eff})$, is defined, for every $k \in \mathbb{R}$, by

$$P(t \leq kt_{eff}) = 1 - e^{-k}. \tag{12}$$

As this probability can be viewed as $\frac{M_{est}(t)}{M^s}$, we have

$$M_{est}(t) = (1 - e^{-\frac{t}{t_{eff}}})M^s, \tag{13}$$

where $M_{est}(t)$ represents an estimation for $M(t)$.

Using the Final Value Theorem, $M^s = \lim_{p \longrightarrow 0} p\overline{M}(p)$, we obtain

$$M^s = -2\ell(2C_{ext} - C^{0g} - C^{0b}). \tag{14}$$

In [21] we deduce an estimation $M_{est}(t)$ for the mass delivered during $[0, t]$,

$$M_{est}(t) = -2\ell(1 - e^{-\frac{t}{t_{eff}}})(2C_{ext} - C^{0g} - C^{0b}). \tag{15}$$

We observe that this estimation avoids the numerical solution of (1). It can be used with (10) as a simple tool to estimate the mass released until a certain time.

In Table III the estimated masses for several times t, computed using (13), are presented.

Table III - Estimated delivery masses.

t	$M_{est}(t)$
t_{eff}	$63.21\%M^s$
$2t_{eff}$	$86.47\%M^s$
$3t_{eff}$	$95.02\%M^s$
$4t_{eff}$	$98.17\%M^s$

In Table IV are presented the estimated delivered masses $M_{est}(t)$, (15), and $M_3(t)$, (5), computed with $D = 0.05$, $\ell = 1$, $\lambda = 0.05$, $C^{0g} = 0.5$, $C^{0b} = 0.5$, $C_{ext} = 0$.

Table IV- Estimated mass and total delivered mass for the therapeutical lens (Model I - System 3)
($D = 0.05$, $\ell = 1$, $\lambda = 0.05$, $C^{0g} = 0.5$, $C^{0b} = 0.5$, $C_{ext} = 0$).

Effective Time	Estimated Mass $M_{est}(t)$	Mass $M_3(t)$	Relative Error
$t_{ef} = 29.15$	$63.21\% M^s = 1.2642$	1.4306919	1.320×10^{-1}
$2t_{ef} = 58.29$	$86.47\% M^s = 1.7294$	1.7825530	3.073×10^{-2}
$3t_{ef} = 87.43$	$95.02\% M^s = 1.9004$	1.9145475	7.445×10^{-3}
$4t_{ef} = 116.57$	$98.17\% M^s = 1.9634$	1.9645691	5.954×10^{-4}

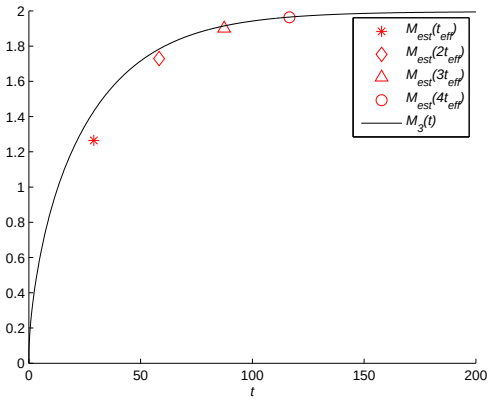

FIGURE 7. Mass tracking of $M_3(t)$, for parameters in Table III.

The plots of the released mass $M_3(t)$ and the corresponding estimated mass $M_{est}(t)$ for the parameters in Table IV, are represented in Figure 7. The values of $M_3(t)$ have been computed from (5) with 100 terms. As expected when t increases a better approximation $M_{est}(t)$ of $M_3(t)$ is obtained.

Once fixed a certain therapeutic mass and a certain waiting time to reach this mass, the lens can be tailored in order to fullfil these requirements. Let us consider, for example, that D and C^{0g} are free parameters. If we define that at $t_{eff} = 1000$, the released mass should be $M_{est}(4t_{eff}) = 1$, then

$$C^{0g} = 0.484329,\ D = 8.415 \times 10^{-3},$$

where $C^{0b} = 0.025$, $C_{ext} = 0$, $\ell = 1$, $\lambda = 0.01$. If the same therapeutic mass is to be delivered within a shorter period of time, $t_{eff} = 100$, then as expected the diffusion coefficient increases, obtaining in this case $D = 1.774 \times 10^{-2}$. The change in drug delivery coefficient can be achieved by manipulating the polymer struture.

2.1.3. *Numerical simulations* versus *experimental results.* To manipulate analytically the equations in model (1) the diffusion coefficient was considered constant. A more realistic model must include the concentration dependence of the diffusion coefficient D.

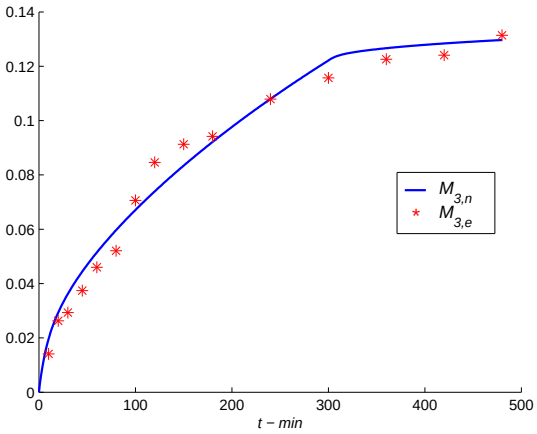

FIGURE 8. Numerical ($M_{3,n}$) and experimental ($M_{3,e}$) mass delivery from a lens with dispersed drug and entrapped particles loaded with drug (System 3) during the first 8 hours.

In Figure 8 we present the numerical released masses from System 3 - the lens with particles - and the experimental masses for the first eight hours. In the computations the following values of the parameters were considered:

$$\begin{aligned} &C^{0b} = 0.05102, C^{0g} = 0.28, \\ &\alpha_1 = 0.01, \lambda = 0.02 \end{aligned} \tag{16}$$

and

$$D(t) = \begin{cases} 0.1996 \times 10^{-3}, \ t \in [0, 300], \\ \\ 0.11 \times 10^{-4}, \ t \in (300, 480]. \end{cases} \tag{17}$$

In Figure 9 we plot the results obtained from System 3 using experimental values and numerical simulations for a period of eight days. The simulations have been carried with the parameters defined in [8] and the diffusion coefficient given by

$$D(t) = \begin{cases} 0.1996 \times 10^{-3}, \ t \in [0, 420] \\ \\ 0.9 \times 10^{-5}, \ t \in (420, 11520] \end{cases} . \tag{18}$$

To represent more realistically the exterior concentration we defined $C^E(t) = \gamma_1 u(-\ell, t)$ with $\gamma_1 = 0.5$. We observe that (16), (17) and (18) are experimental values.

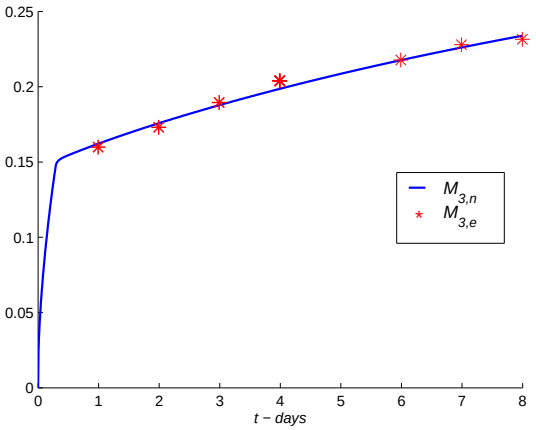

FIGURE 9. Comparison of delivered numerical ($M_{3,n}$) and experimental ($M_{3,e}$) masses for System 3.

2.2. A sandwich type lens. A different mechanism to induce delay in drug delivery from therapeutic lenses has been presented in [13]. The idea lies in creating sandwich type structures composed by three polymeric layers as represented in Figure 1: two non biodegradable layers (HEMA) coating a biodegradable PLGA film containing drug (Model II). As no analytical manipulations were carried on, diffusion coefficients have been represented by more realistically non linear functions. The behavior of the drug release is modeled by the coupled diffusion-reaction system of partial differential equations:

HEMA layer

$$\begin{cases} \dfrac{\partial C^1}{\partial t} = \dfrac{\partial}{\partial x}(D_1(C^1)\dfrac{\partial C^1}{\partial x}),\ x \in (0,\ell_1),\ t>0 \\ C^1(x,0) = 0,\ x \in (0,\ell_1) \\ D_1\dfrac{\partial C^1}{\partial x}(0,t) = \alpha(C^1(0,t) - C^E),\ t>0 \\ D_1\dfrac{\partial C^1}{\partial x}(\ell_1,t) = D_2\dfrac{\partial C^0}{\partial x}(\ell_1,t),\ t>0 \end{cases}, \tag{19}$$

PLGA film

$$\begin{cases} \dfrac{\partial C^0}{\partial t} = \dfrac{\partial}{\partial x}(D_2 \dfrac{\partial C^0}{\partial x}) + c_0 \gamma e^{-\gamma t},\ x \in (\ell_1, \ell_2),\ t > 0 \\ C^0(x,0) = C_0^0,\ x \in (\ell_1, \ell_2) \\ C^0(\ell_1, t) = \beta C^1(\ell_1, t),\ t > 0 \\ D_2 \dfrac{\partial C^0}{\partial x}(\ell_2, t) = D_1 \dfrac{\partial C^2}{\partial x}(\ell_2, t),\ t > 0 \end{cases}, \tag{20}$$

HEMA layer

$$\begin{cases} \dfrac{\partial C^2}{\partial t} = \dfrac{\partial}{\partial x}(D_1(C^2) \dfrac{\partial C^2}{\partial x}),\ x \in (\ell_2, \ell_3),\ t > 0 \\ C^2(x,0) = 0,\ x \in (\ell_2, \ell_3) \\ C^2(\ell_2, t) = \beta C^0(\ell_2, t),\ t > 0 \\ -D_1 \dfrac{\partial C^2}{\partial x}(\ell_3, t) = \alpha(C^2(\ell_3, t) - C^E),\ t > 0 \end{cases}, \tag{21}$$

where $D_1(C) = D_{1e} e^{\beta_1 (1 - C/C_0^0)}$ and $D_2(t) = D_{2e} e^{-\beta_2 e^{-\gamma t}}$.

In (19)-(21) C^1 and C^2 represent the drug concentration in the non biodegradable layers, C^0 represent the drug concentration in the biodegradable PLGA film, D_{1e} and D_{2e} stand for the initial diffusion coefficients in HEMA and PLGA, respectively. We note that ℓ_i are the thicknesses of the different layers, C_0^0 and c_0 are the free and bound initial concentrations in PLGA, respectively. Parameters α and β are related with the flux conditions at the boundary and at the interfaces, respectively; β_1 and β_2 are positive parameters. We assume that binding is not significant in HEMA layers.

The authors in [13] also report experiments carried with a different type of sandwich structure: two HEMA layers linked by a void space containing drug (Model III). The kinetics of the release can be described by equations (19), (21) and an evolution equation in the void space of type

$$\begin{cases} \dfrac{\partial C^{vs}}{\partial t} = -\dfrac{1}{\epsilon} \left[D_1 \dfrac{\partial C^1}{\partial x}(\ell_1, t) + D_1 \dfrac{\partial C^2}{\partial x}(\ell_1 + \epsilon, t) \right],\ x \in (\ell_1, \ell_2),\ t > 0 \\ C^{vs}(0) = C_0^{vs} \end{cases}, \tag{22}$$

where C^{vs} represents the drug concentration in the void space, C_0^{vs} the initial concentration and $\epsilon = \ell_2 - \ell_1$ stands for thickness of the void space between the two HEMA layers.

In Table V we present the description of the three types of lens we have presented so far.

Table V: Description of the models.

Models	Definition	Main equations
Model I - System 3	Lens with particles encapsulating drug	(1)
Model II	Lens of "sandwich" type	(19),(20), (21)
Model III	Lens of "sandwich" type with a void cavity	(19),(22), (21)

We note that model I (System 3) corresponds to the lens described in section 2.1. We present in Figure 10 the plots of the total released masses, corresponding to models I, II and III with boundary conditions of type (4) that simulate *in vitro* results.

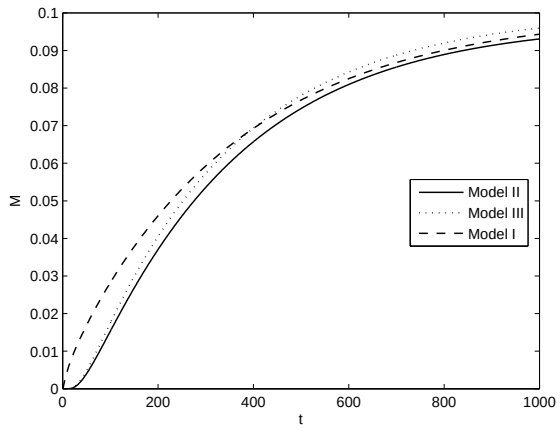

FIGURE 10. Comparison of Models I, II and III.

We considered $C^E = 0$, $\alpha = 0.01$, in all simulations and the values of the parameters exhibited in Table VI. If the drug is entrapped in a single non biodegradable layer where particles are dispersed (model I - System 3) the release is faster than in models II and III in a first period. Afterwards the plot corresponding to model III cross the plot of model I. We remark that "sandwich platforms" with a biodegradable layer - model II - lead to a slower drug release than "non sandwich platforms" - model I.

Table VI: Parameters used in the simulations of Figure 10.

Models	Parameters
Model I	$D = 0.005$, $\lambda = 0.05$, $C^{0b} = 0.01$, $C^{0g} = 0.04$, $\ell = 1$
Model II	$D_{1e} = 0.005$, $D_2e = 0.03$, $\beta_1 = 0.002$, $\beta_2 = 0.001$, $\gamma = 0.01$, $c_0 = 0.01$, $C_0^0 = 0.09$, $\ell_1 = \ell_2 = \ell_3 = 1$
Model III	$D_{1e} = 0.005$, $\beta_1 = 0.002$, $C_0^{vs} = 0.1, \ell_1 = \ell_3 = 1$

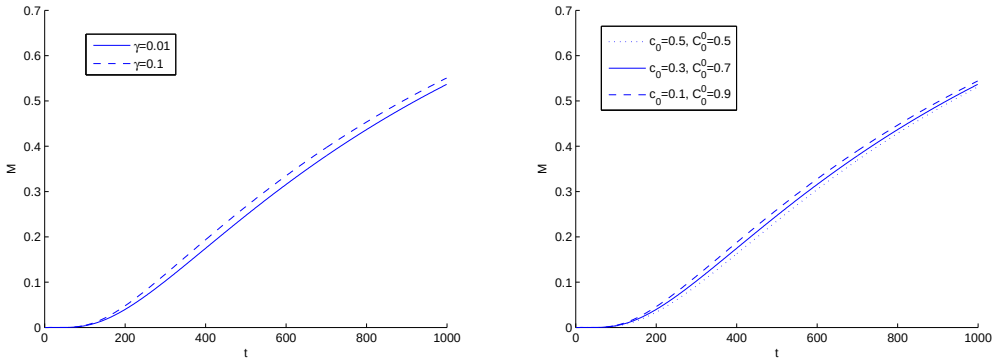

FIGURE 11. A comparison of released mass from the "sandwich" lens (model II) for two different degradation coefficients γ (with $c_0 = 0.3$, $C_0^0 = 0.7$) -left- and different free and bound initial concentration -right- (with $\gamma = 0.1$).

In Figure 11-left- we plot the total released mass of model II for two different degradation coefficients, and in Figure 11-right- we illustrate the behaviour of released mass for different free and bound initial concentration. In these simulations the following values were used: $C^E = 0$, $D_{1e} = 0.001$, $D_{2e} = 0.02$, $\alpha = 0.01$, $\beta_1 = 0.02$, $\beta_2 = 0.02, \ell_1 = \ell_2 = \ell_3 = 1$. From the figure in the left we conclude that the delivered mass is an increasing function of γ. In fact as the polymer erodes the bound drug is free to diffuse through the HEMA layers and the largest is the degradation rate the fastest is the release. The influence of initial concentration is also illustrated in the right of Figure 11: for each t the total released mass is a decreasing function of the initial bound mass. We observe that the values used for the parameters do not correspond to physical values.

We compare now experimental results with numerical simulations obtained with model II.

In Figure 12 numerical simulations of model II are compared with laboratorial results in [13]. We consider $C^E = 0$, $D_{1e} = 0.8554$, $D_{2e} = 4.2336 \times$

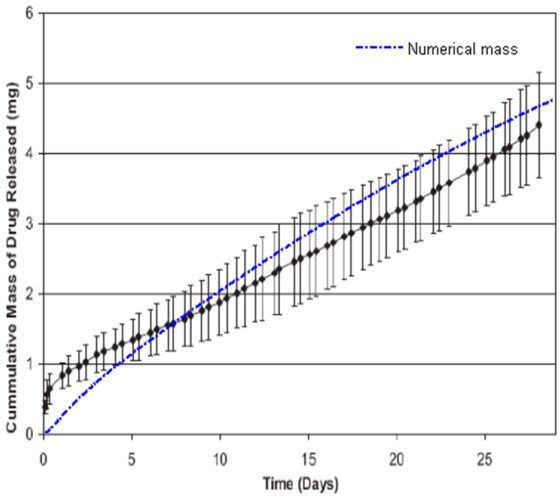

FIGURE 12. Comparison of delivered numerical and experimental masses for "sandwich" type lens (model II).

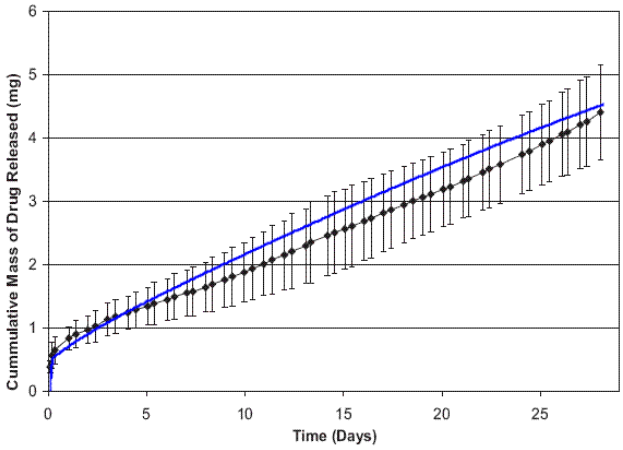

FIGURE 13. Comparison of delivered numerical and experimental masses for "sandwich" type lens (model II).

10^{-7}, $\alpha = 0.5$, $\beta_1 = 1.5$, $\beta_2 = 0.1$, $\gamma = 0.0714$, $c_0 = 0.03475$, $C_0^0 = 0.1$, $\ell_1 = 0.02$, $\ell_2 = 0.01$, $\ell_3 = 0.02$. As referred in [13] after 30 days the lens is still releasing drug. The qualitative behaviour of the numerical prediction shows a good agreement after day 5. We note that the experimental results exhibit an initial burst that is not present in the numerical solution. This is a point deserving some attention. In fact if there was no drug at all in the HEMA layers as reported in [13] this initial burst would not be expectable. This argument suggests that the non biodegradable layers are not

completely drug free. In fact, if we consider that $C^1(x,0) \neq 0,\ x \in (0,\ell_1)$ and $C^2(x,0) \neq 0,\ x \in (\ell_2,\ell_3)$ we obtain the result presented in Figure 13, where a numerical initial burst does not occur.

3. Simulating *in vivo* drug release from therapeutic lens

To have a prediction of the drug concentration in the anterior chamber of the eye we couple the systems representing the delivery from a therapeutic lens with the uptake in living tissues.

The eye is divided into anterior and posterior chamber (Figure 2). The anterior chamber is the front portion of the eye containing aqueous fluid. It is bounded in front by the cornea and in the back by the iris and the lens. The posterior chamber is the space behind the iris, lens and ciliary body. In Section 3.1 the release from a therapeutic lens is compared with the behaviour of an instilled drop. In Section 3.2 the anatomy of the anterior chamber is included in the model and a pathological situation - the obstruction of Schlemm canals - is analyzed.

3.1. Diffusion in the cornea and anterior camera: therapeutic lens versus topical drops. We consider now the coupling of equations representing the diffusion in the lens, in the cornea and the evolution in the anterior chamber. In this model it is assumed that there is no convection of the aqueous humor. To model the diffusion of drug from a therapeutic lens through the cornea to the anterior chamber we consider equations (1) with $D = D_g$, in the domain $(-\ell_1, 0)$.

The behavior of the drug concentration in the cornea, C^c, is described by

$$\frac{\partial C^c}{\partial t} = D_c \frac{\partial^2 C^c}{\partial x^2} - K_c C^c,\ x \in (0,\ell_2), t > 0, \tag{23}$$

where D_c stands for the diffusion coefficient in the cornea and K_c represents a coefficient that takes into account the metabolic consumption.

The conservation of drug in the anterior chamber, C^a, is described by ([15])

$$\frac{dC^a}{dt} = \frac{1}{V_a}\Big(- D_c f_c A_c \frac{\partial C^c}{\partial x}(\ell_2, t) - Cl_a C^a(t)\Big), \tag{24}$$

where A_c is the surface area of the cornea, f_c represents the fraction of A_c occupied by the diffusional route considered and V_a is the distribution volume of solute in the anterior chamber.

Equations (1), (23) and (24) are coupled with the initial conditions

$$C^g(x,0) = C^{0g},\ C^b(x,0) = C^{0b},\ x \in [-\ell_1, 0], \tag{25}$$

$$C^c(x,0) = 0,\ x \in [0, \ell_1], \tag{26}$$

$$C^a(0) = 0, \tag{27}$$

and the boundary conditions

$$\frac{\partial C^g}{\partial x}(-\ell_1, t) = 0, t > 0, \tag{28}$$

$$D_g f_g A_g \frac{\partial C^g}{\partial x}(0,t) = D_c f_c A_c \frac{\partial C^c}{\partial x}(0,t), t > 0, \tag{29}$$

$$C^g(0,t) = K_{g,c} C^c(0,t), t > 0, \tag{30}$$

$$-D_c f_c A_c \frac{\partial C^c}{\partial x}(\ell_2, t) = K_{c,a}\Big(C^c(\ell_2,t) - C^a(t)\Big), t > 0. \tag{31}$$

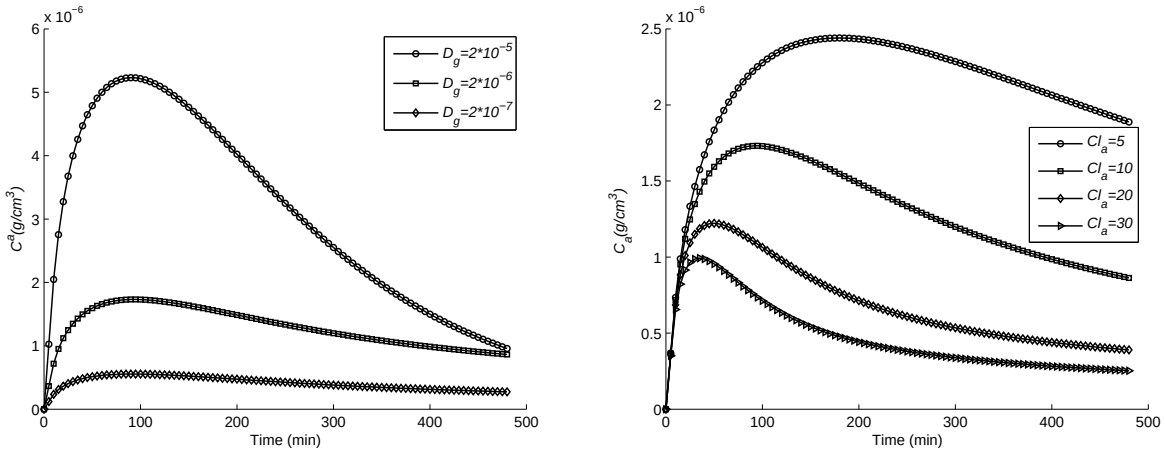

FIGURE 14. Drug concentration in the anterior chamber C^a for different values of the diffusion coefficient in the lens (right) and for different values of the clearance in the anterior chamber (left).

In (29) f_g represents the fraction of the lens surface A_g that is occupied by the diffusional route. The constant $K_{g,c}$ ((30)) represents the quotient of the distribution coefficient in the lens and the cornea and the parameter $K_{c,a}$ represents a volumetric rate.

The dependence of C^a on the diffusion coefficient of the drug in the therapeutic lens is illustrated in Figure 14-left. As the drug diffusion coefficient

in the lens increases, an increasing of the drug concentration in the anterior chamber is observed as expected.

An increasing of the drug clearance in the anterior chamber produces a decreasing of the drug concentration in this compartment. This behavior is illustrated in Figure 14-right.

To compare the efficiency of therapeutic lens with topical eye drops we replaced the delivery from a therapeutical lens by equation ([9])

$$\frac{dC_f}{dt} = \frac{D_c f_c A_c \frac{\partial C^c}{\partial x}(0,t) - SC_f}{V_H + V_i e^{-K_d t}}, \tag{32}$$

where C_f denotes the drug concentration in the tear film and S represents a (fixed) lacrimal secretion rate. In (32) k_d denotes the drainage constant, V_L and V_i represent the normal lacrimal volume and the initial tear volume after an instillation of drug. The previous equation is coupled with the differential equations (2), (3), initial conditions (26), (27),

$$C_f(0) = C_f^0, \tag{33}$$

and with the boundary condition (31). The same assumption is considered in the mathematical model of topical administrations introduced in [16] and considered later in [15]. The coupling between the drug evolution in the tear film and in the cornea is defined by

$$-D_c f_c A_c \frac{\partial C^c}{\partial x}(0,t) = K_{c,a}\Big(C_f(t) - C^c(0,t)). \tag{34}$$

In Figure 15 we plot the time evolution of drug concentration in the anterior chamber when a drop (C^a_{drop}) and a lens (C^a_{lens}) are used in drug administration. In the computation of $C^a_{drop}(t)$ the following parameters

$$k_d = 1.45,\ C_f^0 = 0.5 \times 10^{-3},\ V_L = 7, V_i = 10,\ S = 1.2$$

are used ([15], [16]).

From Figure 15 we conclude that the use of therapeutic lens leads to a higher concentration of the drug in the anterior chamber during a larger period of time than topical administrations. We observe that whereas using a therapeutic lens the drug concentration is significant after 8 hours, when a drop is instilled in the eye the drug concentration vanishes after some minutes.

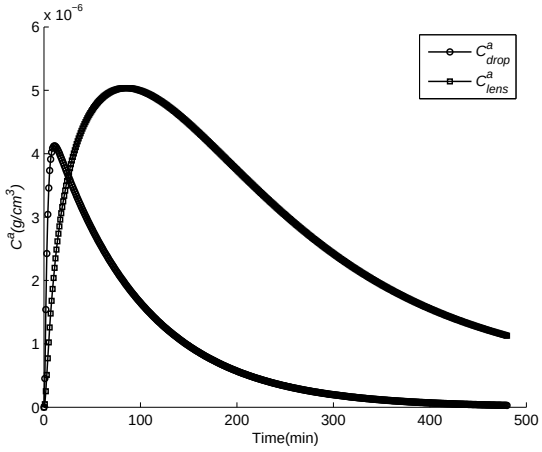

FIGURE 15. Evolution of the drug concentration in the anterior chamber when a drop (C^a_{drop}) and a lenses (C^a_{lens}) are used in the eye drug administration.

3.2. Convective flow in the anterior chamber of the eye. In this section we describe very briefly the release of drug from a therapeutic lens, considering the convection of aqueous humour in the anterior chamber. A complete study of the problem is presented in [20]. The anterior chamber is modeled using real dimensions. The domain is divided into three subdomains (see Figure 16): the therapeutic lens, Ω_1, where equations (1) hold; the cornea, Ω_2, where the drug concentration is described by (23); and the anterior chamber, Ω_3, where the convection-diffusion-reaction equation

$$\left\{ \frac{\partial C_a}{\partial t} = D_a \Delta C_a - \overrightarrow{v}.\nabla C_a - \frac{Cl_a}{V_a} C_a,\ \Omega_3,\ t > 0\ , \right. \tag{35}$$

is coupled with Navier Stokes equations. Initial, interface and boundary conditions complete the model. In (35) D_a denote the diffusion coefficient in the anterior chamber, $\overrightarrow{v}$ the velocity of the aqueous humour, Δ the Laplace operator and ∇ the gradient operator. As mentioned before the use of therapeutic lens is particulary important in the case of severe diseases characterized by high I.O.P.. The intraocular pressure can be explained by obstruction of Schlemm canals, (see Figure 2 and Figure 18) or high rates of aqueous humor production. To simulate a pathological situation we consider a geometry with obstructed Schlemm canals. In our simulations this obstruction induces a high I.O.P. of mean value $30\, mmHg$, whereas a normal value lies in the

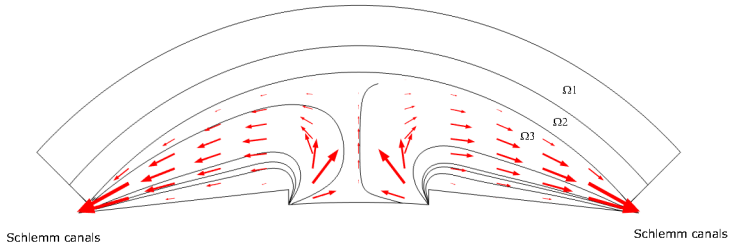

FIGURE 16. Geometry of the therapeutical lens, cornea and anterior chamber.

interval $[15, 20]$. To simulated the aqueous humour we considered an incompressible fluid ($\nabla \overrightarrow{v} = 0$) and we used the density and viscosity of water.

In order to illustrate the evolution of drug concentration, we plot in Figure 17 its value at $t = 20\,min$ in (top) and at $t = 2\,hour$ in (down). Two types of gray scales have been used: a scale in the left for the concentration of drug in the lens and cornea and a scale in the right to represent the drug concentration in the anterior chamber. We note that, as defined in the scale, the lowest levels of drug concentration correspond to dark gray. When we compare these plots we can see that, as expected, the drug concentration decreases with time. In Figure 18 we want to illustrate the influence of the production rate of the aqueous humour in the behaviour of drug concentration. We represent the drug concentration at $t = 1\,h$, in the pathological situation described before; in Figure 18- top - a normal rate was considered whereas in Figure 18- down - the rate was doubled. We note that the increase in rate not only increases the I.O.P. ($27,48\,mmHg$ to $40,39\,mmHg$) but also leads to lowest values in drug concentration (see scale in Figure 18).

4. Conclusion

We presented in this paper an overview of controlled drug delivery from therapeutic lens to the anterior chamber. Mathematical models for *in vitro* delivery of different therapeutic lens were considered and numerical simulations were compared with laboratorial experiments. A time constant - effective time- was introduced and it was shown how it can be used as a tool to help in the design of therapeutic lens with predefined delivery profiles.

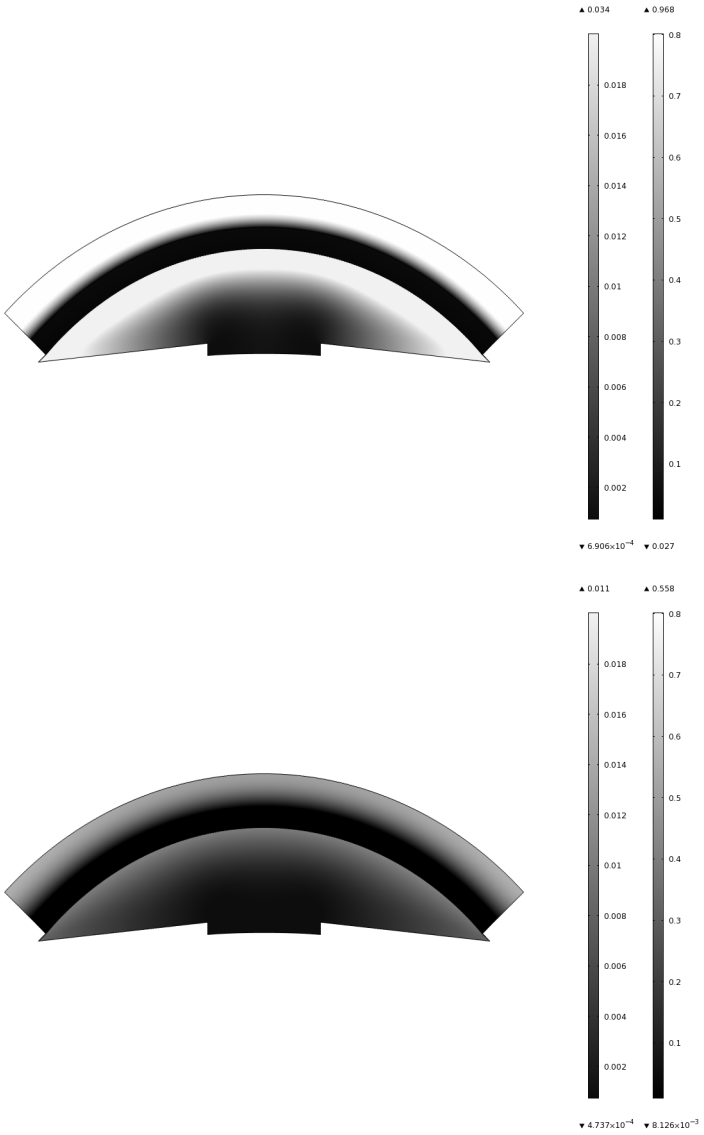

FIGURE 17. Drug concentration at $t = 20\,min$ -(top) and $t = 2\,h$ -(down).

Mathematical models that represent *in vivo* delivery have also been considered. The effectiveness of controlled drug administration *versus* topical drops, has been established.

To model pathologic situations - as the obstruction of Schlemm canals or an increase in the rate of production of aqueous humour - a more complex model is introduced in Section 3.2. A complete study of the model is presented in [20].

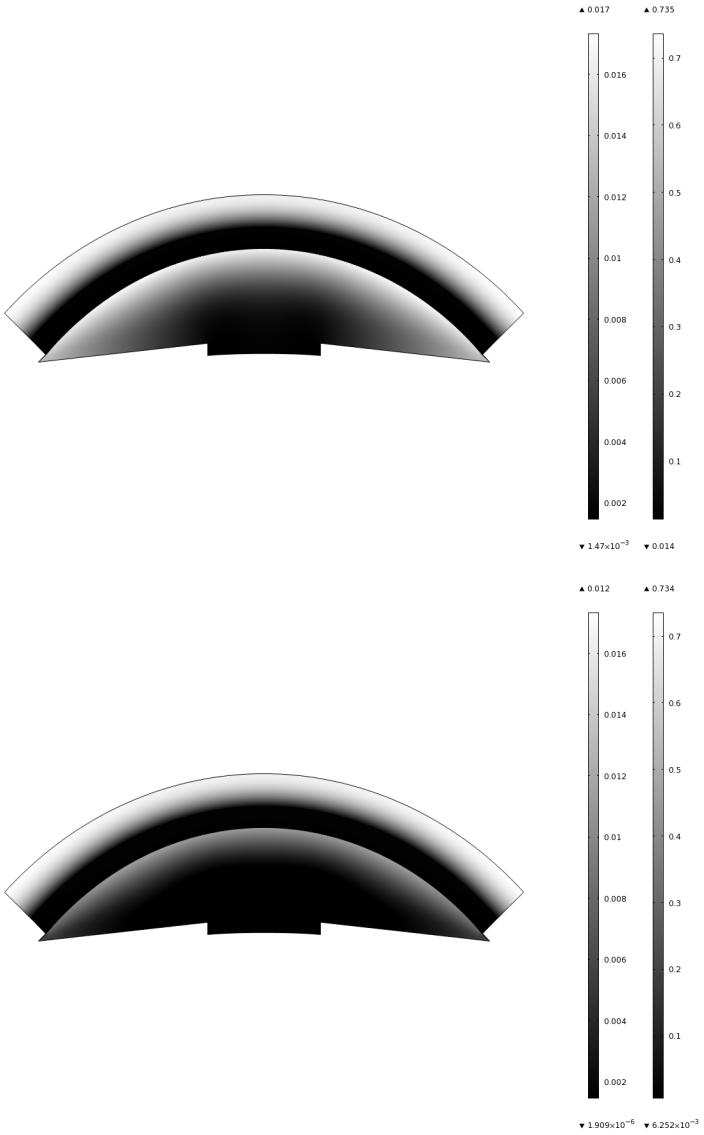

FIGURE 18. Influence of the production rate on the distribution of drug concentration at $t = 1\,h$.

5. Appendix

Symbol	Definition (unities)
D	diffusion coefficient of the drug in the polymeric matrix (cm^2/min)
D_c	diffusion coefficient in the cornea (cm^2/min)
D_a	diffusion coefficient in the anterior chamber (cm^2/min)
C^g	drug concentration in the gel (g/cm^3)
C^b	drug concentration in the particles (g/cm^3)
λ	transfer coefficient (min^{-1})
C^{0g}	initial concentration in the gel (g/cm^3)
C^{0g}	initial concentration in the particles (g/cm^3)
C^E	external concentration (g/cm^3)
α_1	transference coefficient (cm/min)
M	exact solution for the total released mass (g)
$M_i, i = 1, 2, 3, 4$	represent the delivery mass for the Systems 1, 2, 3 and 4 (g)
$M_{3,n}$, $M_{3,e}$	delivered numerical and experimental masses for System 3 (g)
γ_1	rates distribution

C^1, C^2	drug concentration in the non biodegradable layers (g/cm^3)
C^0	drug concentration in the biodegradable layer (g/cm^3)
D_{1e}, D_{2e}	initial diffusion coefficients in HEMA and PLGA (cm^2/min)
$\ell_i, i = 1, 2, 3$	thicknesses of the different layers (mm)
C_0^0, c_0	free and bound initial concentrations in PLGA (g/cm^3)
α, β, β_1, β_2	positive parameters
C^{vs}	the drug concentration in the void space in sandwich platform (g/cm^3)
C_0^{vs}	the initial concentration in the void space (g/cm^3)
C^c	drug concentration in the cornea (g/cm^3)
C^a	drug concentration in the anterior chamber (g/cm^3)
$K_{g,c}$	quotient of the distribution coefficient in the lens and the cornea
$K_{c,a}$	volumetric rate (cm^3/min)
K_c	metabolic consumption drug coefficient in the cornea
ℓ_2	cornea thickness (mm)
V_a	distribution volume of solute in the anterior chamber (μl)
Cl_a	clearence in the anterior chamber $(\mu l/min)$
A_c	surface area of the cornea (cm^2)
f_c	fraction of the cornea surface occupied by the diffusional route
C_f	drug concentration in the tear film (g/cm^3)
S	lacrimal secretion rate $(\mu l/min)$
k_d	drainage constant (min^{-1})
V_L	normal lacrimal volume in tear film (μl)
V_i	initial tear volume after an instillation of drug (μl)
C^a_{drop}	drug concentration in the anterior chamber when a drop is used (g/cm^3)
C^a_{lens}	drug concentration in the anterior chamber when a lens is used (g/cm^3)
v	velocity of the aqueous humour (mm/s)
$M_{est}(t)$	represents an estimation for $M(t)$
t_{eff}	effective time

Acknowledgements

This research was supported by the Centre for Mathematics of the University of Coimbra and Fundação para a Ciência e a Tecnologia, through European program COMPETE/FEDER and by the FCT Research Project UTAustin/MAT/0066/2008.

References

[1] Bourlais, C. L., Acar, L., Zia, H., Sado, P.A., Needham, T., Leverge, R., Ophthalmic drug delivery systems–Recent advances, Progress in Retinal Eye Research, 17, 33-58, 1998.

[2] Hehl, E.M., Beck, R., Luthard, K., Guthoff, R., Drewelow, B., Improved penetration of aminoglycosides and fluorozuinolones into the aqueous humour of patients by means of Acuvue contact lenses, European Journal of Clinical Pharmacology, 55, 317-323, 1999.

[3] McNamara, N.A., Polse, K.A., Brand, R.J., Graham, A.D., Chan, J.S., Mckenney, C.D., Tear mixing under a soft contact lens : effects of lens diameter, American Journal of Ophthalmology, 127, 659-665, 1999.

[4] Nakada, K., Sugiyama, A., Process for producing controlled drug-release contact lens and controlled drug-release contact lenses thereby produced. United States Patents 6, 027, 745, 1998.

[5] Elisseeff, J., McIntosh, W., Anseth, K., Riley, S., Ragan, P., Langer,R., Photoencapsulation of chondrocytes in poly(ethylene oxide)-based semiinterpenetrating networks, Journal of Biomedical Materials Research, 51, 164-171, 2000.

[6] Gulsen, D.; Chauhan, A., Ophthalmic drug delivery from contact lenses, Investigative Ophthalmology and Visual Science, 45, 2342-2347, 2004.
[7] Gulsen, D.; Chauhan, A., Dispersion of microemulsion drops in HEMA hydrogel: a potential ophthalmic drug delivery vehicle, International Journal of Pharmaceutics, 292, 95-117, 2005.
[8] Ferreira, J. A., Oliveira, P., Silva, P. M., Carreira, A., Gil, H., Murta, J. N., Sustained drug release from contact lens, Computer Modeling in Engineering and Science, 60, 152-179, 2010.
[9] Ferreira, J. A.; Oliveira, P.; Silva, P. M.; Murta, J. N., Drug delivery: from a ophthalmic lens to the anterior chamber, Computer Modeling in Engineering and Science, 71, 1-14, 2011.
[10] Podual, K., Doyle, F.J., Peppas, N. A., Preparation and dynamic response of cationic copolymer hydrogels containing glucose oxidase. Polymer 41, 3975-3983, 2000.
[11] Scott, R. A., Peppas, N A., Highly crosslinked, PEG-containing copolymers for sustained solute delivery, Biomaterials, 20, 1371-1380, 1999.
[12] Silva, P.M., Controlled Drug Delivery: Analytical and Numerical Study, *Phd-Thesis*, University of Coimbra, Portugal, 2010.
[13] Ciolino, J. B., Hoare, T. R., Iwata, N. G., Behlau, I., Dohlman, C. H., Langer, R.; Kohane, D.S., A Drug-Eluting Contact Lens, Investigative Ophthalmology & Visual Science, 50, 7: 3346, 2009.
[14] Ferreira, J. A., Oliveira, P., Silva, P. M., A mathematical kit for simulating drug delivery through polymeric membranes, CMMSE 2011, Volume II, edt. J. Vigo Aguiar, 496-507, 2011.
[15] Avtar R., Tandon D., Modeling the drug transport in the anterior segment of the eye, European Journal of Pharmaceutical Sciences, 35, 175-182, 2008.
[16] Zhang, W., Prausnitz, M.R., Edwards, A., Model for transient drug diffusion across cornea, Journal of Controlled Release, 99, 241-258, 2004.
[17] Worakula, N., Robinson, J.R., Ocular pharmacokinetics/pharmacodynamics, European Journal of Pharmaceutics and Biopharmaceutics, 44, 71-83, 1997.
[18] Collins, R., The choice of an effective time constant for diffusive processes in finite systems, Journal Physics D: Applied Physics, 13, 1935-1947, 1980.
[19] Simon, L., Timely drug delivery from controlled-release devices: Dynamic analysis and novel design concepts, Mathematical Bioscience, 217, , 151-158, 2009.
[20] Ferreira, J. A., Oliveira, P., Silva, P. M., Therapeutic lenses and the mathematics of aqueous humour convection: from health to pathology, submited (2012).
[21] Ferreira, J. A., Oliveira, P., Silva, P. M., Mathematical analysis of waiting time for reaching theraputic effects, Computer Modeling in Engineering and Science, 76, 164-174, 2011.
[22] Heys, J. J., and Barocas, V. H., A Boussinesq model of natural convection in the human eye and the formation of krukenberg's spindle, Annals of Biomedical Engineering, 30, 392-401, 2002.

J.A. Ferreira
CMUC, Department of Mathematics, University of Coimbra, Apartado 3008, EC Santa Cruz, 3001-501 Coimbra, Portugal

E-mail address: ferreira@mat.uc.pt

P. de Oliveira
CMUC, Department of Mathematics, University of Coimbra, Apartado 3008, EC Santa Cruz, 3001-501 Coimbra, Portugal

E-mail address: poliveirt@mat.uc.pt

P. M. da Silva

Department of Physics and Mathematics, ISEC, Rua Pedro Nunes, Quinta da Nora, 3030-199 Coimbra, Portugal

E-mail address: pascals@isec.pt